Structural Engineering and Mechanics, Vol. 7, No. 6 (1999) 575-588
DOI: http://dx.doi.org/10.12989/sem.1999.7.6.575

Prediction of crack trajectory by the boundary element method

M.B. Bush

Department of Mechanical and Materials Engineering, The University of Western Australia, Nedlands, WA 6907, Australia

Abstract. A boundary element method is applied to the analysis of crack trajectory in materials with complex microstructure, such as discontinuously reinforced composite materials, and systems subjected to complex loading, such as indentation. The path followed by the crack(s) has non-trivial geometry. A study of the stress intensity factors and fracture toughness of such systems must therefore be accompanied by an analysis of crack trajectory. The simulation is achieved using a dual boundary integral method in planar problems, and a single boundary integral method coupled with sub-structuring in axisymmetric problems. The direction of crack propagation is determined using the maximum mechanical energy release rate criterion. The method is demonstrated by application to (i) a composite material composed of components having the elastic properties of aluminium (matrix) and silicon carbide (reinforcement), and (ii) analysis of contact damage induced by the action of an indenter on brittle materials. The chief advantage of the method is the ease with which problems having complex geometry or loading (giving rise to complex crack trajectories) can be treated.

Key words: crack trajectory; energy release rate; stress intensity factor; boundary element method; toughness.

1. Introduction

The fracture toughness in a composite material depends on a complicated interaction between a multitude of factors, including the particle shape, volume fraction, interface strength, particle strength and pre-existing flaws. It is now well known, for example, that although the mechanical properties of particulate reinforced metal matrix composite materials are generally better than the properties of the monolithic alloy alone (Karandikar and Chou 1991, Levy and Papazian 1992), the fracture properties are not improved. Indeed, the fracture toughness may be significantly lower than that of the monolithic matrix material (Arsenault *et al.* 1991, Leggoe *et al.* 1996). The failure exhibits many of the characteristics of brittle fracture, due to the presence of weak interfaces, pre-existing flaws and restricted potential for plastic deformation in the matrix.

It follows that analysis of the effects of these factors is an equally complex exercise. To analyse the problem effectively we must track the path of the crack, at each stage checking for the preferred direction of propagation, and then allowing the crack to proceed in that direction. Although several crack trajectory algorithms have been proposed in the literature, previous attempts to deal specifically with the discontinuous composite materials are very scarce. Faber and

† Professor

Evans (1983) presented a theoretical analysis based on the assumption that the crack will run in a straight line from particle to particle and then deflect at the particle. For a variety of ideal particle shapes (spheres, rods, discs), they develop a statistical analysis of the toughening expected due to the crack deflection. The analysis assumes that the crak intercepts particles at predetermined points (the path is determined by the particle orientations). Patton and Santare (1993) considered the question of deflection by combining a complex-variable boundary element analysis with common theories for determination of crack direction to study the path of a crack near an elliptical inclusion within an infinite medium. The presence of the ellipse is automatically taken into account by use of the appropriate Green's function. This would appear to be the first such theoretical study, but is nonetheless limited to a rigid inclusion or a pore embedded in an infinite domain. A somewhat more sophisticated analysis was more recently carried out by Kim *et al.* (1997), who analyse the effects of particle clusters on the toughness of silicon carbide particulate reinforced alumina. They demonstrate the importance of thermally induced residual stresses on the crack behaviour in these systems, however, their analysis does not take into account the elastic mismatch between the phases in the composite. In the present work we consider the effects of elastic mismatch in the absence of residual stresses. The effects of residual stresses are easily included if required (Mammoli and Bush 1995).

All the above studies demonstrate the importance of correctly predicting the crack geometry before any conclusions can be drawn regarding the effective toughness of the material. At a given location of the crack front, calculations must be performed to determine the preferred direction of propagation. The crack is then incremented by a small amount in this direction and the process repeated. Several algorithms of this type have been proposed in the past, using both finite element methods (Brazant *et al.* 1973, Valliapan and Murti 1985, Kocer and Collins 1997) and boundary element methods (Portela *et al.* 1993). A drawback of the finite element approach is the need to re-mesh the problem at every increment of the crack, although much of the additional computational load can be alleviated through the use of a moving patch of elements surrounding the crack tip. The problem of re-meshing does not arise in the boundary element method, making the method very attractive in problems having complex geometry. It must be noted, however, that there may be an additional computational cost associated with the use of this method relative to the finite element method.

In previous studies of crack trajectory, the direction of crack propagation was determined by utilizing information near the crack tip, either by direct examination of the crack tip stress field or through the calculations of strain energy. The strain energy is determined by integration of the stress and strain fields or by evaluation of the J-integral around the crack tip. In the current applications, however, the crack tip may pass very close to an interface in the composite system. Under such conditions, the use of stress fields close to the crack tip may become unreliable. Alternatively, we may evaluate the energy release rate from the work done by the external loads. The direction of maximum energy release rate is determined directly by allowing the crack to propagate in a number of test directions. In this way we directly identify the direction of maximum energy release rate without making any prior assumptions about the system.

2. Formulation

2.1. Boundary element formulation

The dual formulation described by Portela *et al.* (1993) allows the crack problem to be treated

without the need for artificial sub-structuring. Elements are only required on the crack faces and outer boundary of the computational domain. The dual boundary element method is characterised by the use of a pair of integral equations:

$$c_{ij}(P)\,u_j(P)=\int_\Gamma U_{ij}^*(P,Q)\,t_j(Q)\,d\Gamma-\int_\Gamma T_{ij}^*(P,Q)\,u_j(Q)\,d\Gamma \tag{1}$$

and

$$C_{ij}(P)\,t_j(P)=\int_\Gamma D_{ijk}^*(P,Q)\,n_k t_j(Q)\,d\Gamma-\int_\Gamma S_{ijk}^*(P,Q)\,n_k\,u_j(Q)\,d\Gamma \tag{2}$$

where Γ indicates the problem boundary (including the crack faces), $u_j(P)$ and $t_j(P)$ represent the velocity and traction at a boundary node P, n_k is the outward directed normal vector at P and the coefficients c_{ij} and C_{ij} are tensors that depend on the continuity of the surface at P. The functions U_{ij}^*, T_{ij}^*, D_{ijk}^* and S_{ijk}^* are the relevant fundamental solutions, which link together the point P and any other general boundary point Q.

Eq. (2) is obtained by differentiation of Eq. (1). As a result, the functions D_{ijk}^* and S_{ijk}^* are derived by differentiation of U_{ij}^* and T_{ij}^*. In planar or three dimensional problems these functions are all easily defined in analytical form. In an axisymmetric problem, however, the functions U_{ij}^* and T_{ij}^* contain higher transcendental functions. The differentiation of these functions and manipulation to produce D_{ijk}^* and S_{ijk}^* involves a ridiculous amount of algebra. As a result, attempts to produce a set of dual equations analogous to Eqs. (1) and (2) for axisymmetric problems have not been successful. In the current work, the axisymmetric problem has been treated using the single Eq. (1) coupled with domain sub-structuring (the crack lies on a fictitious interface). The resulting formulation, although not as convenient or efficient as a dual formulation, still retains the advantages of the simple mesh structures characteristic of the boundary element method.

Eqs. (1) and (2) are solved in conjunction with appropriate boundary and interface conditions. The boundary conditions consist of prescribed values of displacement or traction components. Each particle is treated as a separate sub-region, with its own set of material properties. If the particle and the matrix are perfectly bonded, then the interface conditions become:

$$t_j^m=-t_j^p,\quad u_j^m=u_j^p \tag{3}$$

where the superscripts 'm' and 'p' refer to the matrix and the particle, respectively. This merely states that forces and displacements are continuous across the interface. If a flaw exists on part of the interface, then the displacement will no longer be continuous. In this case the interface conditions take the form:

$$t_j^m=t_j^p=0,\qquad u_j^m=u_j^p+du_j \tag{4}$$

where du_j is the displacement vector across the flaw. Finally, the crack faces are assumed to be traction free:

$$t_j^1=t_j^2=0,\qquad u_j^1=u_j^2+du_j \tag{5}$$

where the superscripts 1 and 2 refer to the two sides of the crack face.

The application of the method is illustrated in Fig. 1. In the case of the dual equation formulation (planar problems), Eq. (1) is applied to all boundary nodes and the nodes that lie on one side of the crack. Eq. (2) is then applied to nodes that lie on the opposite side of the crack. In the case of the single equation formulation, Eq. (1) is first applied to the sub-region A, followed

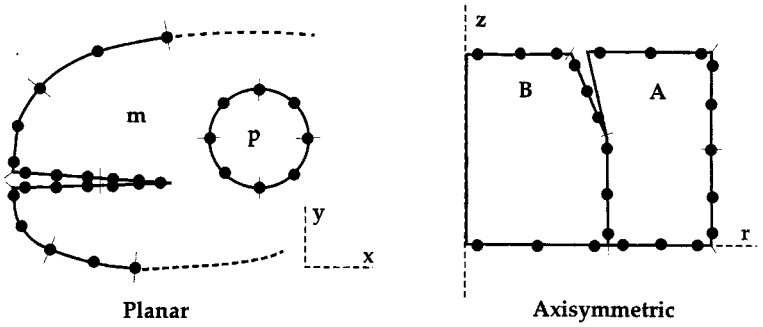

Fig. 1 Example boundary element models of planar (x-y) and axisymmetric (r-z) problems. The filled circles indicate nodes, while the short lines indicate the element end points. The letters 'm' and 'p' refer to the matrix and particle, respectively, while 'A' and 'B' refer to sub-regions

by sub-region B. In this manner a sufficient number of linearly independent equations are developed for the boundary, interface and crack face solution variables.

The equations are converted into discrete form using quadratic, isoparametric boundary elements, as illustrated in Fig. 1. Each element is associated with three nodes, thereby allowing the displacement and traction forces on the element to be represented by quadratic functions. The outer nodes on each element may coincide with the end points of the element, but may also be moved along the element away from the end point to allow for a discontinuity of the function across the element end point. The elements used on the crack faces must be discontinuous to avoid mathematical singularity in the formulation.

2.2. Crack propagation criterion

Most of the proposed criteria for defining the preferred direction of crack propagation fall into two categories: Energy methods and stress methods. Energy methods propose that the crack will propagate in the direction of maximum energy release rate, while the stress methods assume that the crack will propagate in the direction that minimizes the Mode II loading. There appears to be little difference between the predictions obtained by these methods, provided that the mode II loading on the crack is relatively small.

The energy release rate can be determined using a variety of techniques. Firstly, we can directly calculate the work done by external forces as the crack is allowed to propagate a small amount in a chosen test direction. Secondly, we can determine the work of crack closure after propagation in the test direction. Thirdly, the J-integral can be utilized. In the first two cases the direction of maximum energy release rate must be found by repeating the calculation using a number of test kink angles, until the direction of maximum release rate is found. In practice the number of test angles is limited to less than three or four, since the kink angle will be close to zero. Use of the J-integral avoids the need for repeated calculation (Portela *et al.* 1993), but requires further calculation of stresses and strains along the integral path. These calculations can become inaccurate when they are made close to a boundary or the crack tip. Since we wish to allow the crack tip to closely approach the interface between the matrix and reinforcement, we have utilized the first of the approaches described above in the current work.

The process of determining the direction of crack propagation is illustrated in Fig. 2. After the solution corresponding to a particular crack location has been obtained, the potential energy in the

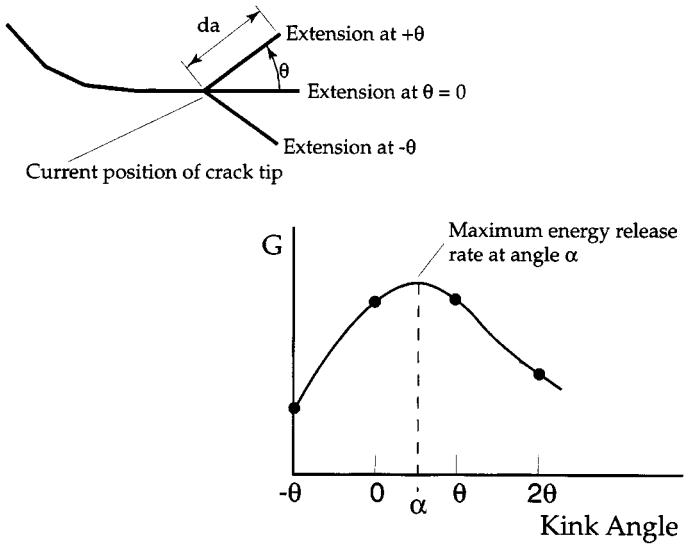

Fig. 2. Procedure for evaluation of the direction of maximum energy release rate

structure is determined by calculating the work done by external forces applied as boundary conditions. The crack is then allowed to propagate by a small amount, *da*, in a chosen direction and the solution repeated. The energy release rate, *G*, is then determined by:

$$G = \frac{|PE_1 - PE_2|}{da} \tag{6}$$

where PE_1 and PE_2 are the potential energies corresponding to the two crack locations. The entire exercise is then repeated for each of a variety of increment angles until the direction of maximum energy release rate has been found. The crack is then propagated in that direction by a prescribed amount, and the process repeated.

The appropriate choice of the crack tip increment, *da*, is considered in the following section,

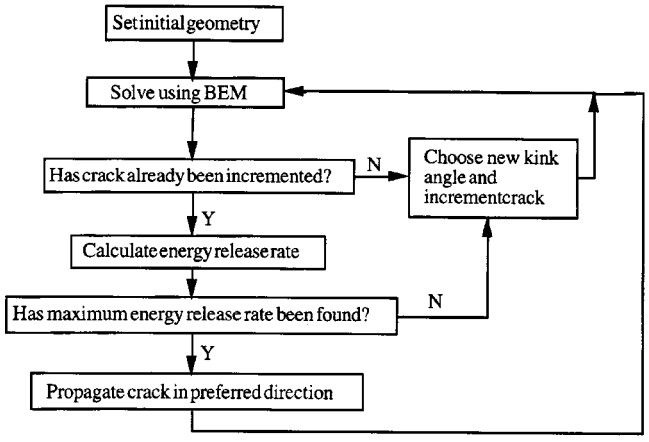

Fig. 3 Algorithm for calculation of crack trajectory

where the solution to a well defined problem is examined. A variety of tests have shown that adequate evaluation of the crack propagation direction can be made using a kink increment of 4 degrees. Interpolation to find the exact angle that maximizes the energy release rate can then be performed accurately. Once the appropriate direction has been determined, the crack is propagated in that direction by an amount typically equal to 3(*da*), although increments as small as (*da*) are used when the rate of change of crack direction is high. In general, however, smaller increments make little difference to the calculated trajectory. The overall algorithm is illustrated in Fig. 3.

3. Energy release rate for a uniformly stressed square plate with an edge crack

The accuracy of the calculated energy release rate obviously depends on the relative size of the crack tip increment. Since the energy release rate is determined by numerical differentiation according to Eq. (6), the accuracy should be increased as the size of the increment is reduced. However, in practice there is also the potential for numerical round-off error to become dominant under these conditions. Although all calculations have been performed using double precision arithmetic to minimize the influence of round-off error, it is nonetheless necessary to systematically assess the effects of the numerical approximations by comparison with the exact solution of a well defined problem. This analysis will provide the basis for choosing appropriate crack tip increment and element numbers in more complex problems.

The geometry of the problem is shown in Fig. 4. A square plate containing a single edge crack is subjected to a uniform traction loading. The exact solution to this problem for various values of a/H is given by (Chivelek and Erdogan 1982). Boundary elements of equal length are used to represent each of the edges of the square. The same number of elements, N_H, is used on each edge. The crack faces are also subdivided into elements of equal length, except for the final 'graded'

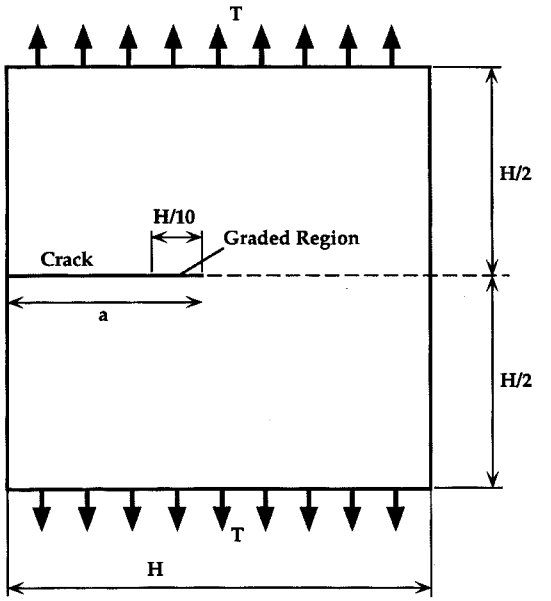

Fig. 4 A square region containing an edge crack of length a. The elements used on the crack faces have equal length, except for a graded region near the crack tip

region, representing a total length of $H/10$. In this region the element lengths are reduced as the crack tip is approached. This is achieved using a geometric scaling factor, SF, in conjunction with the total number of elements in the graded region, N_t. The scaling factor is just the length of one element relative to the length of the adjacent element. The effects of both SF and N_t are investigated below.

In Fig. 5 we see the computed energy release rate, G, plotted against N_t for a plane stress analysis with a/H=0.5 and SF=0.7. The graph also gives the corresponding values of da. The results are presented in non-dimensional form using the exact solution G_{exact}. Very high accuracy can obviously be achieved with relatively few elements. The largest error, corresponding to the use of only four crack tip elements (N_t=4), is just 6 per cent. The accuracy clearly improves as N_t is increased, with less than one per cent error incurred with N_t=8. Although convergence is

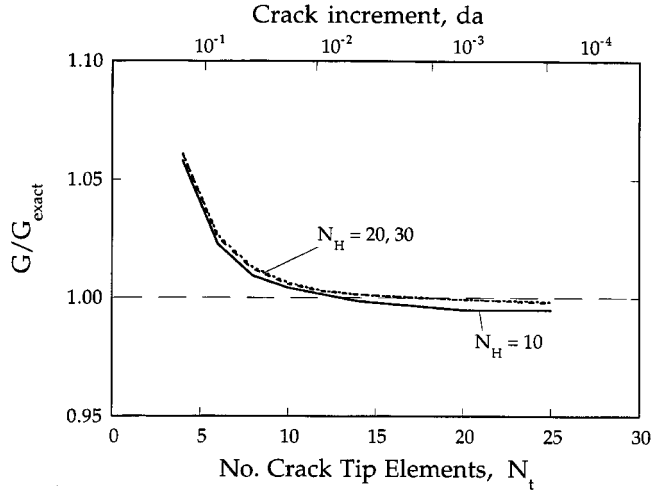

Fig. 5 The dimensionless energy release rate for the problem of Fig. 4, with a/H=0.5. and SF=0.7

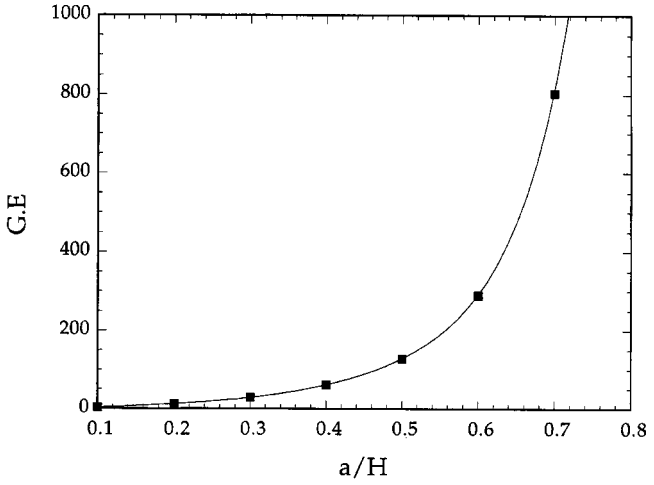

Fig. 6. The product of energy release rate, G, and Elastic modulus, E, for the problem of Fig. 4, with SF= 0.7, N_t=8, and N_H=10. The Solid line is the numerical prediction while the filled symbols represent exact results (Civelek and Erdogan 1982)

observed as N_H is increased, the effect is relatively minor and excellent accuracy is achieved with N_H=10. It is also noteworthy that there is no sign of the onset of round-off error. The effect of the scale factor, SF, was found to be relatively minor, although SF=0.7 yielded the best accuracy. Finally, in Fig. 6 we show the computed energy release rate as a function of a/H. Once again, a high degree of accuracy is maintained as the relative length of the crack is varied.

The results of the above analyses suggest that excellent accuracy can be achieved in this geometry using SF=0.7, N_t=8 and N_H=10. These are typical of the values utilized in all subsequent work. Greater accuracy could be achieved by using more elements, although at the expense of increased computational cost.

4. Crack shielding due to a single particle

An edge crack is allowed to propagate towards a single, centrally located particle contained within a square plate of side length H. The crack is located on the left edge, and the plate is subjected to a uniform traction force applied to the top and bottom edges (see Fig. 4). The particle radius, a, is 0.05H. The co-ordinates are made non-dimensional by dividing by the particle radius. The 'effective' toughness of the composite (K_c) is presented in the form of a toughness 'enhancement', K_c/K_c^0, where K_c^0 is the toughness of the non-reinforced matrix material. It is easily shown that the ratio K_c/K_c^0 is equivalent to $\sqrt{(G_0/G)}$, where G is the actual energy release rate and G_0 is the energy release rate that would exist under the same loading conditions, but in the absence of reinforcing particles.

The properties of the phases were taken to be those of a typical aluminium alloy and silicon carbide: E_p/E_m=6.43, v_p=0.17 and v_m=0.33, where E is the elastic modulus, v is Poisson's ratio and the subscripts p and m refer to the particle and matrix, respectively.

Typical boundary element numbers used in the calculations are 50 on each particle and 20 on each side of the enclosing boundary. Further increases in these values made little difference to the results. Several hundred elements may be used on the crack faces, depending on the length of the

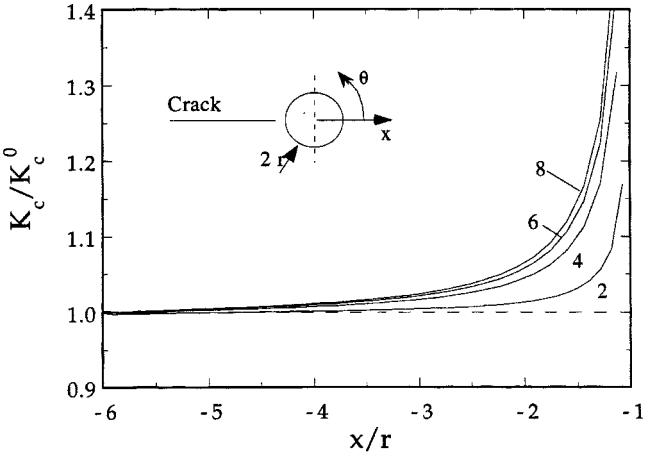

Fig. 7 The composite toughness for a crack approaching a single particle along the centerline, for various values of the stiffness ratio, E_p/E_m

crack. A crack increment, *da*, of approximately 0.0025H was found to give accurate results.

Fig. 7 illustrates the variation of effective toughness as the crack approaches the particle. It is clear that the particle produces substantial crack 'shielding' ($K_c/K_c^0 > 1$), which becomes more important as the ratio of the particle stiffness to matrix stiffness is increased. In the case of Al/SiC, where the ratio of elastic moduli is 6.43, the crack will sense the particle at a distance of at least five particle radii. The results agree with the work of (Li and Chudnovsky 1993), which deals with the interaction between a crack and a particle in an infinite medium.

If the crack is approaching along a path that is offset from the centreline of the particle then it will deflect as it nears the interface. Fig. 8 shows the effect of moving the crack a distance *d* from the particle centreline, and some corresponding trajectories are shown in Fig. 9. It is interesting to note that as the crack approaches the particle it experiences a substantial shielding effect, as expected, but that after it passes the particle an 'amplification' effect occurs ($K_c/K_c^0 < 1$). It is also noteworthy that although the crack 'senses' the presence of the stiff phase at least five radii ahead of the particle, as evidenced by its effect on the toughness, the crack does not experience a substantial deflection until it is within approximately one radius of the interface. As a consequence, the stresses on the interface and within the particle may become relatively large, and this will have corresponding consequences regarding interface failure of particle fracture. This may go part of the way to explain the high incidence of interface and particle failure that has been observed to accompany the fracture of SiC/Al metal matrix composite systems (Leggoe *et al.* 1996). In particular, damage is observed to accumulate some distance ahead of the crack tip.

When interface stresses are sufficiently high to induce fracture, the resulting flaw will then influence the subsequent behaviour of the crack. Such flaws appear to attract the crack (Leggoe *et al.* 1996, Patton and Santare 1993), thereby promoting rapid crack propagation and subsequent fracture of the material. In order to observe the effect of an interface flaw, the case of d/r=0.8 has been repeated, but now a flaw is located between the angular positions θ_1 and θ_2. The angle θ is measured in the anticlockwise sense from the initial crack path (Fig. 7). The cases of a flaw

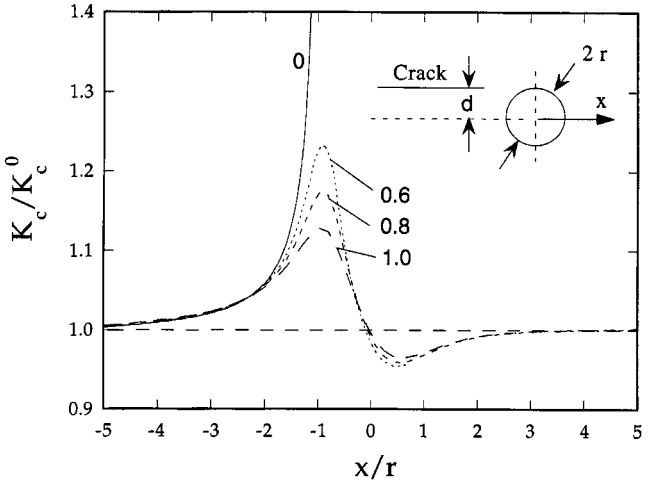

Fig. 8 The composite toughness for a crack approaching a single particle for various values of *d*/*r*. The components of the composite have the elastic paroperties of aluminium (matrix) and silicon carbide (particle)

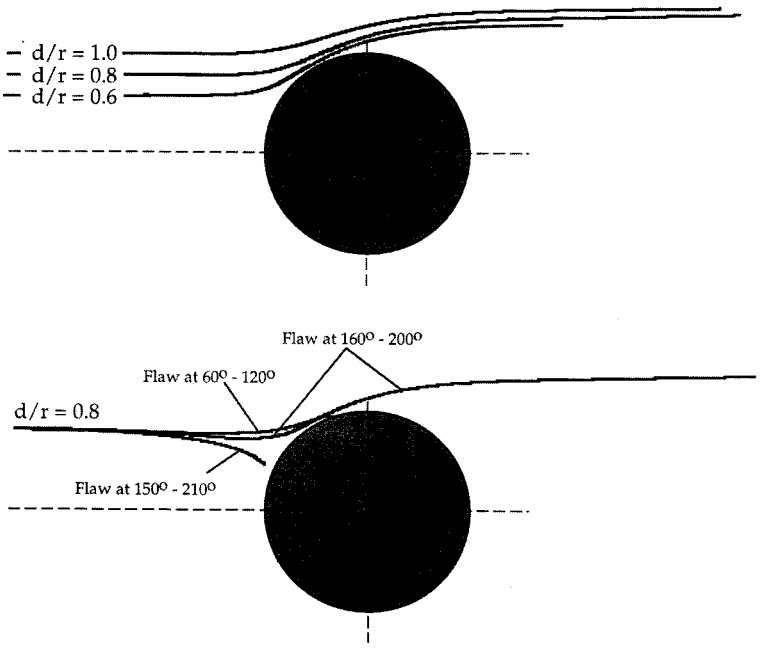

Fig. 9 Computed trajectories for the cases indicated in Fig. 8.

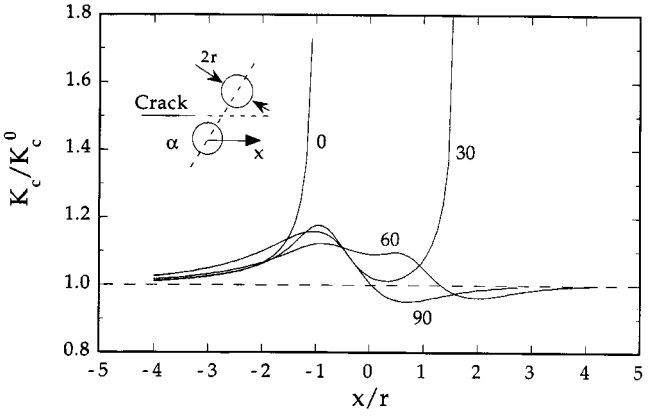

Fig. 10 The composite toughness for a crack approaching a cluster of two equal particles separated by a distance equal to 1r, for various values of the angle α. The initial crack path is equidistant from each particle

centred on the position θ=90 degrees and θ=180 degrees are considered. The resulting trajectories are illustrated in Fig. 9. Although the flaw centered on θ=180 degrees deflects the crack, it does not substantially affect the crack until the extent of the flaw is increased from 40 degrees to 60 degrees. The deflection of the crack path is associated with a dramatic increase in the energy release rate as the ligament of material between the crack tip and the flaw becomes smaller; the crack will rapidly propagate towards the flaw.

5. Crack interaction with a pair of particles

Fig. 10 illustrates the toughness enhancement as the crack approaches and passes the pair of particles with various orientations. Shielding occurs in all cases, particularly when α=0 and 30 degrees, where the crack collides with the particles. When the crack is able to pass between the particles (α>60 degrees) the cluster behaves in a similar fashion to a single particle (but with larger diameter) as the crack approaches. Notice, however, that the maximum degree of shielding occurs when the crack draws approximately level with the first particle (x/a=-1). At some point beyond this position 'amplification' is seen to occur (K_c/K_c^0<1). Both effects are the result of stiffening created by the presence of the particles. Stiffening of the region ahead of the crack reduces the crack opening and hence the energy release rate. Once the crack has passed the particles, however, the region behind the crack tip is now stiffened, leading to increased crack opening. Once the crack is well clear of the particles, the energy release rate returns to the value seen in the unreinforced material (K_c/K_c^0=1).

6. Contact damage due to surface indentation

We now move to an example in which the geometry is simple, but where the loading and stress fields are complicated. Indentation induced damage on the surface of monolithic ceramic materials or ceramic coatings has been used as a simple means of investigating the surface properties of these materials. (See, for example, An *et al.* 1996 and Wuttiphan *et al.* 1996). It is now well known that indentation on a brittle monolith produces a spectacular cone crack, as illustrated in Fig. 11. The angle the crack makes with the surface is a function of the Poisson's ratio. In coarse grained ceramics, indentation may also be associated with quasi-plastic deformation due to the creation and deformation of micro-flaws by shear within the compression zone beneath the indenter. The energy absorption associated with such damage affects the growth of the cone crack, generally leading to suppression of the crack (Lee *et al.* 1997a). Indentation of a stiff coating which is strongly bonded to a compliant substrate usually leads to multiple cone cracks (Lee *et al.*

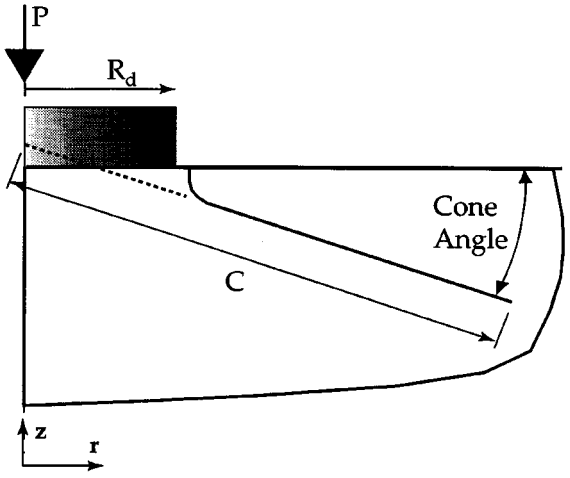

Fig. 11 A cone crack created by the action of a cylindrical indenter

1997b). Cracks are observed to initiate at the surface and extend towards the interface, while other cracks initiate at the interface and extend towards the surface. Additional cracks may initiate within the coating and extend in both directions. However, none of these cracks fully traverses the coating. In particular, the cone cracks extending from the surface show a tendency to deflect away from the interface and eventually cease to propagate as the indentation load is further increased. This is quite contrary to the behaviour observed during indentation of a brittle monolith, where the crack continues to propagate into the material. The phenomenon appears to be intimately linked to the elastic mismatch between the layers, which substantially alters the nature of the stress and strain fields in the coating relative to the case of a monolith.

The problem of cone crack formulation in soda-lime glass has recently been revisited by Kocer and Collins (1997). In particular, they use a finite element analysis to determine the cone crack angle (22°). A significant outcome of this work is the conclusion that the crack trajectory cannot be determined on the basis of the calculated stress field in the absence of the crack, an approach that yields the true cone angle only of the Poisson's ratio is assumed to be 0.33 rather than the actual value of 0.21 (Lawn 1993). In the current example we extend the work of Kocer and Collins to calculate the cone angle as a function of Poisson's ratio. In addition, we have modelled an actual set of experiments to predict the crack length as a function of indenter load.

A boundary element model of the problem shown in Fig. 11 was established using a cylindrical block of material having radius and depth both equal to $20R_d$. A small starting crack ($0.01R_d$) was located at a radius equal to $1.1R_d$. This approximates the experimentally observed behaviour. The starting crack is placed normal to the surface, which again matches experimental observation. Under the action of a given indenter load, the crack first propagates further into the material and then turns away from the compression zone beneath the indenter to finally achieve a given cone angle. Propagation will continue until the energy release rate falls below the critical value determined by the toughness of the material. Increased indenter loading will then force the crack to propagate further. If the trajectory of the crack is all that is required, then it is sufficient to set the toughness to zero and to compute the trajectory under the action of an arbitrary constant indenter load.

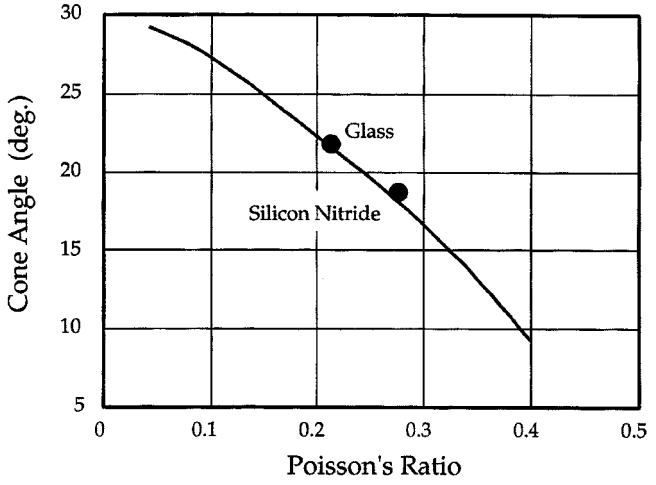

Fig. 12 Predicted cone crack angle as a funtion of Poisson's ratio. The filled symbols are experimental data

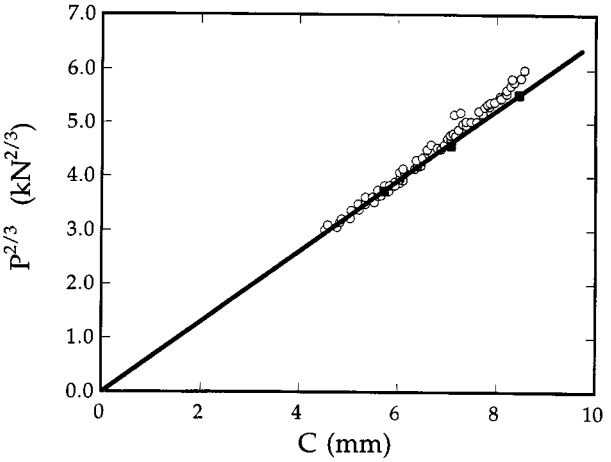

Fig. 13 Calculated crack depth (filled symbols) as a function of indentation load. The solid line represents Eq. (7) fitted to the predicted data. The open symbols are experimental data obtained from Lawn (1993)

The calculated cone angle as a function of Poisson's ratio is shown in Fig. 12, together with the experimental data for soda-lime glass (Lawn 1993) and silicon nitride (Lee *et al.* 1997a). Most brittle materials exhibit a Poisson's ratio between 0.2. and 0.3. No reliable data outside this range is available at the current time.

In the specific case of soda-lime glass we have modelled indentation by an indenter having a radius of 1 mm. The following material properties were adopted: Elastic modulus E=69 GPa, Poisson's ratio ν=0.21, Toughness K_c=0.75 MPa$\sqrt{m}$. Lawn (1993) show that when the crack length is substantially larger than the indenter radius, an asymptotic expression can be used to represent the relationship between crack length and load:

$$C = (\chi/K_c)^{2/3} P^{2/3} \tag{7}$$

where C is the extended crack length shown in Fig. 11 and χ is a function of the Poisson's ratio. Fig. 13 shows the computed relationship between C and $P^{2/3}$ compared to a set of careful experiments (Lawn 1993). The value of χ determined from the slope of the line is 0.045. It is clear that the boundary element model accurately predicts the crack length.

7. Conclusions

(1) A boundary element method for analysis of crack trajectory and energetics in complex problems has been developed. The chief advantage of the method when applied to problems having complex geometry is the ease with which the mesh is updated as the crack grows. The examples presented illustrate that problems involving rapid changes in propagation direction and problems in which the crack passes close to an interface can be handled with equal ease.

(2) The energy release rate is evaluated directly through calculation of the work done by external forces as the crack propagates. The preferred direction of propagation is determined by allowing the crack to proceed in several test directions. We have found this to be a very reliable and robust means of trajectory calculation.

Acknowledgements

Some of this work was carried out while the author was a Guest researcher at the National Institute of Standards and Technology, Gaithersburg, Maryland, U.S.A. The support of the Institute is gratefully acknowledged.

References

An, L., Chan, H.M., Padture, N.P. and Lawn, B.R. (1996), "Damage-resistant alumina-based layer composites", *J. Mater. Res.*, **11**, 204-210.

Arsenault, R.J., Shi, N. and Feng, C.R. (1991), "Localized deformation of SiC-Al composites", *Mater. Sci. Eng.*, **131**, 55.

Brazant, Z., Glazik, J.L. and Achenbach, J.D. (1973), "Elastodynamic fields near running cracks by finite elements", *J. Appl. Mech.*, **105**, 232-236.

Civelek, M.B. and Erdogan, F. (1982), *Int. J. Fract.*, **19**, 139.

Faber, K.T. and Evans, A.G. (1983), *Acta Metall.*, **31**, 565.

Karandikar, P.G. and Chou, T.-W.(1991), *J. Mat. Sci.*, **26**, 2255.

Kim, B.-N., Watanabe, M., Enoki, M. and Kishi, T. (1997), "2-D simulation of crack propagation in A1203 matrix composites dispersed with SiC particles", *Key Engin. Mat.*, **127**, 1153-1158.

Kocer, C. and Collins, R.E. (1997), "The angle of Hertzian cone cracks", *J. Am. Ceram. Soc.*, In Press.

Lawn, B.R. (1993), *Fracture of Brittle Solids*-Second Ed. Cambridge University Press, Cambridge.

Lee, S.K., Wuttiphan, S. and Lawn, B.R. (1997a), "Role of microstructure in Hertzian contact damage insilicon nitride, I: Mechanical characterization", *J. Am. Ceram. Soc.*, **80**, 2367-2381.

Lee, K.S., Wuttiphan, S., Hu, X.-Z., Lee, S.K. and Lawn, B.R. (1997b), "Contact-induced transverse fractures in brittle layers on soft substrates: A study on silicon nitride bilayers", *J. Am. Ceram. Soc.*, in Press.

Leggoe, J.W., Hu, X.Z. and Bush, M.B. (1996), "Crack tip damage development and crack growth resistance in particulate reinforced metal matrix composites", *Eng. Fract. Mech.*, **53**, 873-895.

Levy, A. and Papazian, J.M. (1992), "Tensile properties of short fiber-reinforced SiC/Al composities, Part II: Finite-element analysis", *Metall. Trans. A. Phys. Metall.*, **21**, 411.

Li, R. and Chudnovsky, A. (1993), "Variation of the energy release rate as a crack approaches and passes through an elastic inclusion", *Int. J. Fract.*, **59**, R69-R74.

Mammoli, A.A. and Bush, M.B. (1995), "The effects of reinforcement geometry on the elastic and plastic properties of metal matrix composites", *Acta. Metall. Mater.*, **43**, 3743.

Patton, E.M. and Santare, M.H. (1993), "Crack path prediction near an elliptical inclusion", *Engin. Fract. Mech.*, **44**, 195-205.

Portela, A., Aliabadi, M.H. and Roorke, D.P. (1993), "Dual boundary element integral analysis of crack propagation", *Comp. Struct.*, **46**, 237-247.

Valliapan, S. and Murti, V. (1985), "Automatic re-meshing technique in quasi-static and dynamic crack propagation", *Proceedings of NUMETA '85*, Swansea, January.

Wuttiphan, S., Lawn, B.R. and Padture, N.P. (1996), "Crack suppression in strongly-bonded homogeneous/heterogeneous laminates: A study on glass/glass-ceramic bilayers", *J. Am. Ceram. Soc.*, **79**, 634-640.